Topological magnetic order and superconductivity in $EuRbFe_4As_4$

M. Hemmida,[1,*] N. Winterhalter-Stocker,[2,*] D. Ehlers,[1] H.-A. Krug von Nidda,[1] M. Yao,[3] J. Bannies,[3,†] E. D. L. Rienks,[4] R. Kurleto,[5,6] C. Felser,[3] B. Büchner,[5,7] J. Fink,[5,3,7] S. Gorol,[2] T. Förster,[8] S. Arsenijevic,[8] V. Fritsch,[2] and P. Gegenwart[2]

[1]*Experimental Physics V, Center for Electronic Correlations and Magnetism, University of Augsburg, D-86135 Augsburg, Germany*
[2]*Experimental Physics VI, Center for Electronic Correlations and Magnetism, University of Augsburg, D-86135 Augsburg, Germany*
[3]*Max Planck Institute for Chemical Physics of Solids, D-01187 Dresden, Germany*
[4]*Helmholtz-Zentrum Berlin, Albert-Einstein-Strasse 15, D-12489 Berlin, Germany*
[5]*Leibniz Institute for Solid State and Materials Research Dresden, Helmholtzstr. 20, D-01069 Dresden, Germany*
[6]*M. Smoluchowski Institute of Physics, Jagiellonian University, Łojasiewicza 11, PL-30-348, Kraków, Poland*
[7]*Institut für Festkörperphysik, Technische Universität Dresden, D-01062 Dresden, Germany*
[8]*Hochfeld-Magnetlabor Dresden (HLD-EMFL) and Würzburg-Dresden Cluster of Excellence ct.qmat, Helmholtz-Zentrum Dresden-Rossendorf, D-01328 Dresden, Germany*

(Received 6 October 2020; revised 26 March 2021; accepted 27 April 2021; published 6 May 2021)

We study single crystals of the magnetic superconductor $EuRbFe_4As_4$ by magnetization, electron spin resonance (ESR), angle-resolved photoemission spectroscopy, and electrical resistance in pulsed magnetic fields up to 63 T. The superconducting state below 36.5 K is almost isotropic and is only weakly affected by the development of Eu^{2+} magnetic order at 15 K. On the other hand, for the external magnetic field applied along the *c* axis the temperature dependence of the ESR linewidth reveals a Berezinskii-Kosterlitz-Thouless topological transition below 15 K. This indicates that Eu^{2+} planes are a good realization of a two-dimensional *XY* magnet, which reflects the decoupling of the Eu^{2+} magnetic moments from superconducting FeAs layers.

DOI: 10.1103/PhysRevB.103.195112

I. INTRODUCTION

Magnetic superconductors and superconducting magnets are very intriguing materials due to the competition of magnetic order and superconductivity. Theoretical predictions made by Ginzburg showed that uniform magnetism in bulk compounds may destroy superconductivity due to the electromagnetic mechanism [1]. For example, the incompatible nature of superconductivity and ferromagnetism was demonstrated by experiments, which showed the competition of the two collective phenomena in (La,Gd) and (Ce,Pr)Ru_2 solid solutions [2]. The suppression of ferromagnetism in the superconducting regime was explained by Anderson and Suhl in terms of the Ruderman-Kittel-Kasuya-Yosida (RKKY) interactions by the end of the 1950s [3]. Judging from the energy scale, however, ferromagnetism wins over superconductivity in most cases. Thus, it was suggested that in the superconducting state, the spin susceptibility is suppressed at small wave vectors and pure ferromagnetism should be modified in the form of crypto-ferromagnetic alignment for localized spins [3]. Only in the late 1970s the coexistence of superconductivity and ferromagnetism was evidenced in $ErRh_4B_4$ [4] and $Ho_{1.2}Mo_6S_8$ [5] in narrow regimes of temperature and external magnetic field. In the late 1990s, superconductivity and weak ferromagnetism were observed in high-temperature superconductor rutheno-cuprates [6,7]. In the examples above, superconductivity and ferromagnetism obviously originate from different electrons of different elements. However, there is a scenario that both superconductivity and ferromagnetism arise from the same type of electrons: e.g., in UGe_2 [8] and URhGe [9] the superconductivity emerges from the ferromagnetic background ($T_c < T_m$), where T_m is the magnetic transition temperature. Such compounds are called superconducting magnets, while magnetic superconductors are known for the case of $T_c > T_m$.

Contrary to bulk materials, the coexistence of superconductivity and ferromagnetism may easily be achieved in artificially fabricated superconductor/ferromagnet heterostructures. Due to the proximity effect the Cooper pairs penetrate into the ferromagnetic layer giving the unique possibility to study properties of superconducting electrons under the influence of the huge exchange field. The proximity effect at superconductor/ferromagnet interfaces produces a damped oscillatory behavior of the Cooper pair wave function within the ferromagnetic medium [10]. In inhomogeneous superconductivity, an analogous effect was predicted a long time ago which is well known as the Fulde-Ferrel-Larkin-Ovchinikov (FFLO) effect [11,12]. This effect first was suggested for a pure ferromagnetic superconductor at low temperatures. Moreover, by variation of the nanoscale thickness of the ferromagnetic and superconducting layers in a controllable manner it is possible to change the relative strength of the two competing ordering mechanisms [13,14].

[*]These two authors contributed equally.
[†]Present address: Quantum Matter Institute, University of British Columbia, Vancouver, BC V6T 1Z4, Canada.

Fe-based superconductors are characterized by multiband superconductivity as well as high transition temperatures. These features make it possible to see new phenomena including those due to the interplay of superconductivity and magnetism [15]. Evidence of the coexistence of superconductivity and ferromagnetism was observed, for example, in $SrFe_2As_2$ [16] due to the lattice distortions. Coexistence of superconductivity and ferromagnetism was also observed in other iron-pnictide systems like $Sr_2VFeAsO_3$ [17] and $CeFe(As_{1-x}P_x)O_{0.95}F_{0.05}$ [18] where it results from vanadium and Ce ions, respectively.

An outstanding example comes from Eu-based iron pnictides, especially $EuFe_2As_2$-related systems, in which the Eu^{2+} ions show large local magnetic moments with $J = S = 7/2$. The Eu^{2+} magnetic moments in $EuFe_2As_2$ are coupled ferromagnetically within the *ab* planes, but antiferromagnetically along the *c* axis. It means that Eu^{2+} magnetic moments are rotated by 180° from plane to plane [19]. The compound undergoes a spin-density-wave (SDW) order in the Fe sublattice accompanied by a tetragonal-to-orthorhombic structural phase transition below $T_{SDW} = 195$ K [20]. Substitution of Fe place with Ru [21,22] or Ni [23] in $EuFe_2As_2$ suppresses the SDW transition. This process is accompanied by the appearance of superconductivity or the absence of it for Ru and Ni doping, respectively. Both cases are associated with the emergence of ferromagnetic ordering of Eu^{2+} magnetic moments. Ferromagnetic ordering of Eu^{2+} magnetic moment in $EuFe_2As_2$ was also achieved by the substitution of As place with the isoelectronic element P [24]. It was found that with increasing P substitution, the Eu^{2+} magnetic moments tilt out of the *ab* plane, yielding a net ferromagnetic component along the *c* direction. Moreover, the coexistence of superconductivity and ferromagnetism due to the chemical substitution was observed and confirmed by various methods [21,25–34].

Very recently, new members of the iron-pnictide family, the so-called 1144-system $ABFe_4As_4$ (A = Ca, Sr, Ba, Eu; B = K, Rb, Cs) realize the coexistence of ferromagnetism and superconductivity [35–39]. In $EuRbFe_4As_4$, the Eu^{2+} magnetic moments align ferromagnetically within the *ab* planes, but rotate by 90° from plane to plane along the *c* axis [40]. On the other hand, $EuRbFe_4As_4$ undergoes a superconducting transition above the magnetic one ($T_c > T_m$). These findings motivated intensive theoretical [41–45] and experimental [40,46–61] works in order to understand the interplay between these two antagonistic phenomena.

In this comprehensive study, we report synthesis of single crystalline samples of $EuRbFe_4As_4$ and their magnetic and transport characterizations. Also we outline experimental details of electron spin resonance (ESR), resistivity at high-magnetic fields, and angle-resolved photoemission spectroscopy (ARPES). The analysis of ESR data shows that the spin dynamics of Eu^{2+} ions is ascribed to the Berezinskii-Kosterlitz-Thouless scenario. On the other hand, the analysis of upper critical field data reveals an almost isotropic superconductivity. The noninteraction or rather the weak interaction between conduction electrons of FeAs layers and localized Eu^{2+} magnetic moments is also discussed in the frame of ESR and ARPES results.

II. EXPERIMENTAL DETAILS

Single crystals of $EuRbFe_4As_4$ were grown using FeAs flux with the same method described by Meier *et al.* for the synthesis of $CaKFe_4As_4$ [62]. Via mechanical cleaving the crystals can be removed out of the matrix of FeAs flux and potential $RbFe_2As_2$ and $EuFe_2As_2$ foreign phases can be eliminated. With this method very thin crystal plates can be extracted with lateral dimension up to 2 mm × 4 mm. The crystal plate equates the *ab* plane and the tetragonal *c* axis is perpendicular to this plane.

Magnetization measurements were performed using a commercial magnetometer (Quantum Design MPMS3) at temperatures $2 \leqslant T \leqslant 300$ K and in external magnetic field of 10 Oe. Samples were measured on heating following the zero-field-cooled (ZFC) as well as field-cooled (FC) measurement protocol.

The resistivity was measured on single crystals in steady magnetic fields up to 14 T (1 T = 10^4 Oe) for $2 \leqslant T \leqslant 300$ K using a physical properties measurement system (Quantum Design PPMS) with the electrical transport option ($\nu = 117$ Hz). For these measurements platelike crystals with lateral dimensions up to 2 mm x 4 mm were employed. Utilizing a four-point probe the sample was connected via silver epoxy to Pt wires. Furthermore, measurements at high magnetic fields up to 63 T were carried out using a nondestructive pulsed-field coil at the Dresden High Magnetic Field Laboratory.

ESR measurements were performed in a continuous wave spectrometer (Bruker ELEXSYS E500) at X- and Q-band frequency ($\nu = 9.35$ GHz and 34 GHz, respectively) in the temperature region $4 \leqslant T \leqslant 300$ K using a continuous He gas-flow cryostat (Oxford Instruments). ESR detects the power P absorbed by the sample from the transverse magnetic microwave field as a function of the static magnetic field H. The signal-to-noise ratio of the spectra is improved by recording the derivative dP/dH using a lock-in technique with field modulation.

ARPES measurements were conducted at the 1^3-ARPES end station attached to the beamline UE112 PGM at BESSY, equipped with a Scienta R4000 energy analyzer. All data presented in this contribution were taken at temperatures between 1 and 50 K. The achieved energy and angle resolutions were between 4 and 10 meV and 0.2°, respectively. Polarized photons with energies $h\nu = 20$-130 eV were employed to reach different k_z values in the BZ and spectral weight with a specific orbital character [63,64]. Inner potentials between of 12 and 15 eV were used to calculate the k_z values from the photon energy.

III. EXPERIMENTAL RESULTS AND DISCUSSION

A. Structure and magnetic characterizations

The sample quality was confirmed by means of x-ray diffraction (XRD) analysis. In Fig. 1(a) the room-temperature XRD pattern is shown. The presence of the $h + k + l =$ odd peaks indicates the ordered $P/4mmm$ structure, because these peaks would be forbidden in the $I4/mmm$ order of the 122-structure. There is no visible signature of $EuFe_2As_2$ and

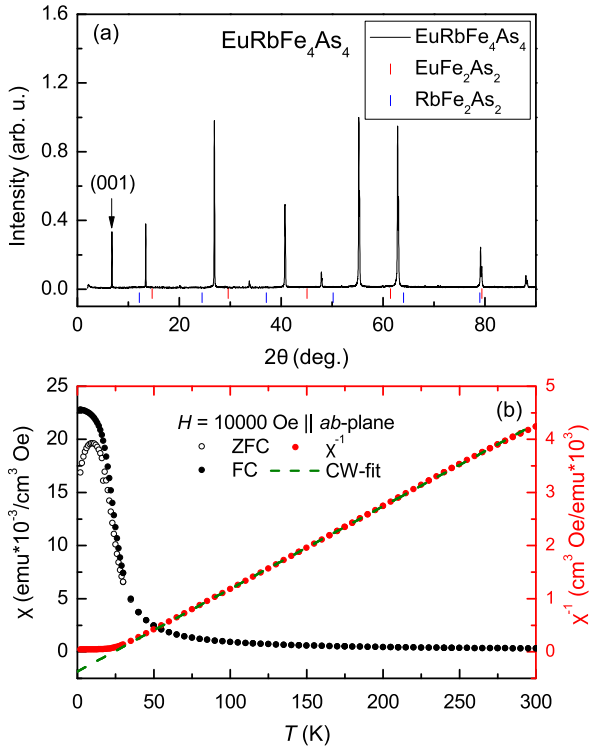

FIG. 1. (a) Diffractogram of $EuRbFe_4As_4$ with the marked peak positions of $RbFe_2As_2$ and $EuFe_2As_2$. A clear peak at low angle marks the characteristic (001) reflection. (b) Temperature dependence of the magnetic susceptibility measured in a field of 10 000 Oe for $H||ab$. The open symbols show the ZFC measurement and the closed symbols the FC measurement. The red data points correspond to the red axis at the right side and show $1/\chi$. This data show the Curie-Weiss-like behavior at high temperatures with a Curie-Weiss temperature of $\Theta_{CW} = 24.7$ K and an effective moment of $\mu_{eff} \approx 7.98\mu_B$/f.u..

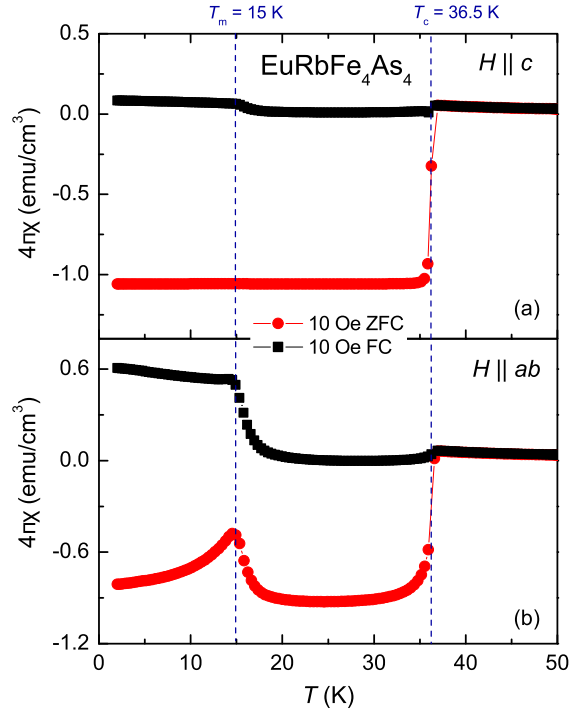

FIG. 2. Temperature dependence of magnetic susceptibility $\chi = M/H$ of $EuRbFe_4As_4$ in a field of 10 Oe applied along the c axis and the ab plane as shown in (a) and (b), respectively. The red data points correspond to the *ZFC* measurement and the black ones to the *FC* measurements. From these measurements a superconducting transition temperature $T_c = 36.5$ K can be determined. The Eu^{2+} magnetic moments order ferromagnetically at $T_m = 15$ K.

$RbFe_2As_2$ $(00l)$ peaks which are the most common impurity phases. The peak positions are in good agreement with the lattice constants reported by Bao *et al.* [39] ($a = 0.38825$ nm, $c = 1.32733$ nm).

In Fig. 1(b) the temperature dependence of the magnetic susceptibility $\chi = M/H$ for $H||ab$ at 10000 Oe is shown. The compound is dominated by the Curie paramagnetic contribution of the localized Eu^{2+} moments ($J = S = 7/2$). The positive value of Curie-Weiss temperature $\Theta_{CW} \approx 25$ K indicates the predominant ferromagnetic nature of the exchange interaction. The effective moment was determined as a mean value of the effective moments of different directions to be $\mu_{eff} = 7.98\mu_B$/f.u.. This value is close to the theoretical value $\mu_{eff} = g\mu_B\sqrt{J(J+1)} \approx 7.94\mu_B$/f.u., which confirms the 2+ state of europium in $EuRbFe_4As_4$.

A field of 10 Oe was applied along the c axis and within the ab plane [see Figs. 2(a) and 2(b)]. At 36.5 K a sharp downturn marks the superconducting phase transition. The diamagnetic signal for $H||c$ is close to $4\pi\chi = -1$ and indicates a complete superconducting volume. At $T_m = 15$ K a kinklike anomaly in the ZFC measurement indicates the ordering of Eu^{2+} within the superconducting state. In contrast to $H||ab$, the magnetic signal at $T_m = 15$ K is only marginal. This is an indication that Eu^{2+} moments prefer the ab plane as an easy plane and hence represent a good realization of the two-dimensional XY model. In the ab plane the FC measurement shows only a small kink at T_c which indicates the transition. This is due to the fact that in the FC condition the flux is frozen in the sample and no complete Meissner state can be established.

Figure 3 shows ESR spectra of $EuRbFe_4As_4$ below, near, and above $T_c = 36.5$ K in the paramagnetic regime for the magnetic field aligned along different crystallographic directions. All spectra in this regime exhibit a single exchange-narrowed resonance which is well described by an asymmetrical Lorentz line due to the skin effect. The skin effect appears in metals because of the interaction between the applied microwave field and mobile charge carriers. This leads to an admixture of dispersion χ' to the absorption χ'' depending on the ratio of skin depth and sample size [65]. The ratio χ'/χ'' is found to change from 0.1 above T_m to values slightly larger than 1 above T_c (paramagnetic metal).

In the vicinity of T_c, the ESR spectra show nonresonant absorption (front peaks or bumps) due to the surface resistivity [66]. As the temperature increases and the system reaches T_c the front peak disappears and the system becomes a conventional paramagnetic metal. As the linewidth ΔH is large enough and comparable to the order of magnitude of the resonance field H_{res}, the counter-resonance at $-H_{res}$ was considered in the fit [67]. The g factor at high temperatures is close to 2 for both $H||ab$ and $H||c$. The resonance field shifts

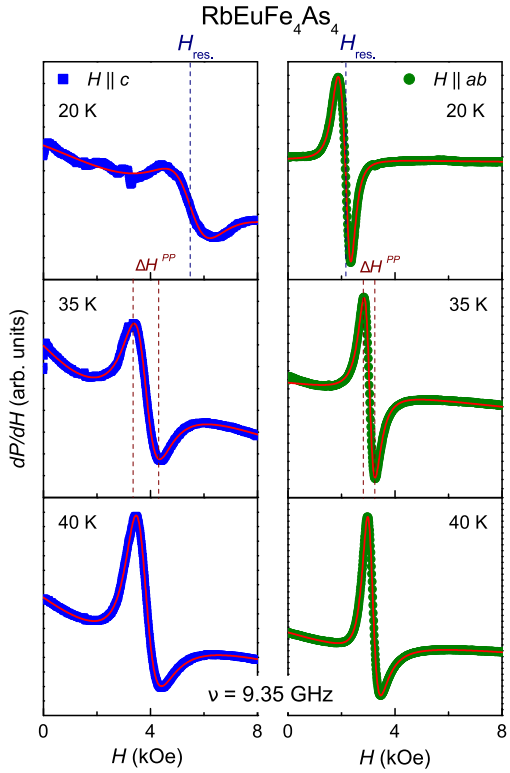

FIG. 3. ESR spectra in the X band ($\nu = 9.35$ GHz) for selected temperatures in the paramagnetic regime of $EuRbFe_4As_4$ along and perpendicular to the c axis below, near and above $T_c = 36.5$ K in the paramagnetic regime. The resonance field $H_{res.}$ and the linewidth (peak-to-peak) ΔH^{PP} are marked on the spectra at 20 K and 36 K, respectively. The resonance field $H_{res.}$ is centered at $\omega = \gamma H_{res.}$ with a half width at half maximum (HWHM) linewidth $\Delta H = \frac{\sqrt{3}}{2}\Delta H^{PP} = 1/\gamma T_2$ where $\gamma = g\mu_B/\hbar$ and T_2 is the spin-spin relaxation time. The solid line indicates the fit with the field derivative of an asymmetric Lorentz line.

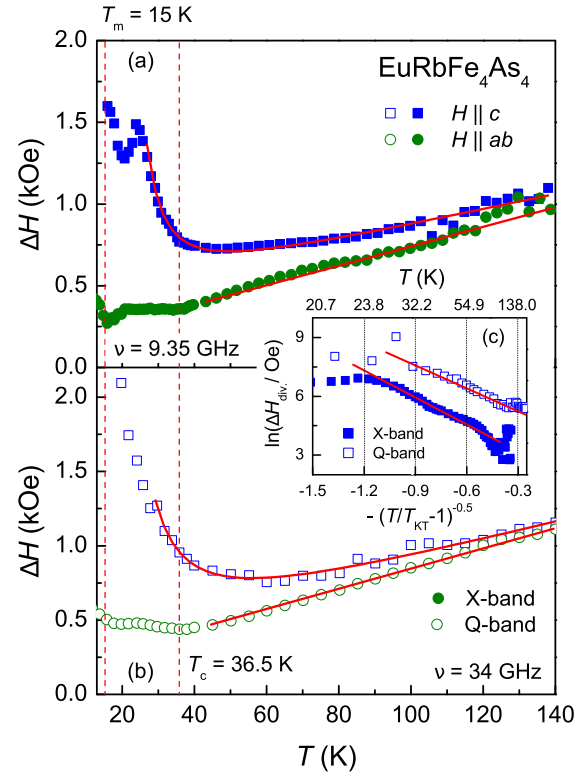

FIG. 4. Temperature dependence of the ESR linewidth of $EuRbFe_4As_4$ measured at the X band (panel (a), $\nu = 9.35$ GHz) and Q band (panel (b), $\nu = 34$ GHz). Dashed vertical lines indicate T_m and T_c. Solid lines represent a combined formula of Korringa and BKT formulas for $H||c$: $mT + \Delta H_\infty \exp[3b/\sqrt{\frac{T}{T_{KT}} - 1}] + \Delta H_0$ where ΔH_0 is the residual linewidth. The inset (c) shows the quality of the BKT fit using logarithmic plot $\ln(\Delta H_{div})$ vs the reduced temperature $-(T/T_{KT} - 1)^{-0.5}$; $\Delta H_{div} = \Delta H_\infty \exp[3b/\sqrt{\frac{T}{T_{KT}} - 1}] - mT - \Delta H_0$. The corresponding real temperature values are depicted in the upper axis of the inset. For $H||ab$ only linear Korringa fit is applied for $T > 40$ K.

to the lower (higher) field for $H||ab$ ($H||c$) on approaching magnetic order on account of demagnetization effects due to the thin plate shaped sample (Fig. 3). However, taking into account the demagnetization factor by means of the Kittel's formula [68], the corrected g factor near 4 K is estimated as $g_{ab} = 2.068$ and $g_c = 2.023$.

The most important information is obtained from the temperature dependence of the linewidth (Fig. 4). The linewidth ΔH increases strongly upon approaching the magnetic transition $T_m = 15$ K from above. On the other hand, ΔH starts to increase linearly with temperature above $T_c = 36.5$ K as well. This indicates the dominant role of the Korringa relaxation of the localized Eu^{2+} spins via scattering of the conduction electrons:

$$\Delta H = \frac{\pi k_B}{g\mu_B}\langle J^2(q)\rangle D^2(E_F)T = mT, \qquad (1)$$

where $\langle J^2(q)\rangle$ is the squared exchange constant between localized spins and conduction electrons averaged over the momentum transfer q, $D(E_F)$ is the conduction-electron density of states at Fermi energy E_F, and m is the Korringa slope [65,69]. A typical value of m in Eu-based iron pnictides is about 8 Oe/K [33,70–72]. This value is typical of the S state of $4f^7$ local moments in conventional metals as well [65,69,73].

According to Willa *et al.* in Ref. [52], specific heat measurements under magnetic field along the c axis up to 3 kOe reveal a topological phase transition—the so-called Kosterlitz-Thouless phase transition—at $T_{KT} \approx 9$ K. This finding was confirmed by Monte Carlo simulations of an easy-plane two-dimensional Heisenberg model. Following these results, one can apply a Berezinskii-Kosterlitz-Thouless (BKT) scenario [74–76] in order to describe the relaxation mechanism of the ESR linewidth at low temperatures ($T < 60$ K) for $H||c$. It implies that

$$\Delta H = \zeta^3 = \Delta H_\infty \exp\left[3b/\sqrt{\frac{T}{T_{KT}} - 1}\right], \qquad (2)$$

where ζ is the correlation length of vortices above T_{KT}, ΔH_∞ is the ESR linewidth in high-temperature approximation (neglecting any Korringa relaxation), and $b = \pi/2$ for the square lattice (see, e.g., Ref. [77]).

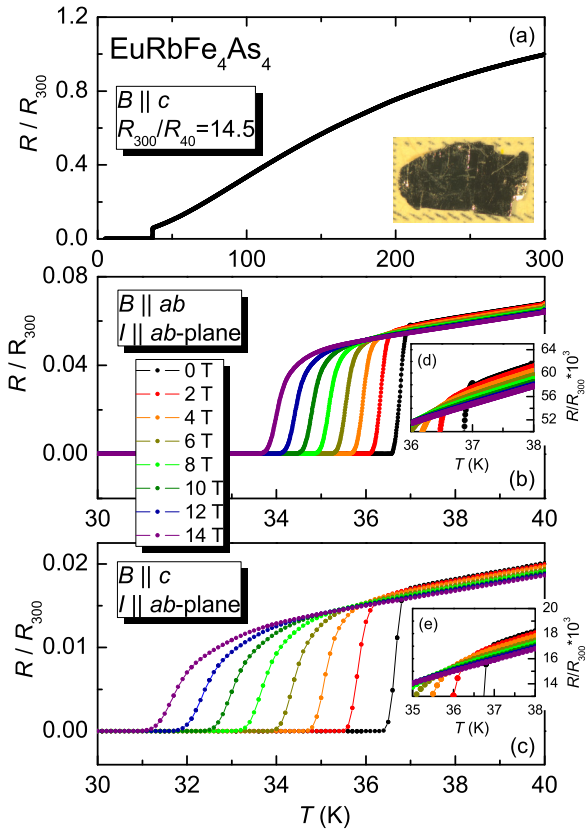

FIG. 5. (a) Normalized in-plane resistance (I || ab plane). The measurement shows a convex curvature. The inset depicts the single crystal under investigation. (b) Shift of the transition in fields up to 14 T with the field applied within the ab plane. (c) Shift of the superconducting transition in fields up to 14 T applied along the c axis. Inset panels (d) and (e) are showing the enlarged resistivity curves across superconducting transition temperatures.

One obtains $T_{KT} \approx 14$ K and 11 K for the X and Q bands, respectively, which are in fair agreement with values reported in Ref. [52]. The value of T_{KT} is always below the magnetic ordering temperature T_m, observed in zero-field ($T_{KT}/T_m \approx 0.7 - 0.9$), as typically found in quasi-two-dimensional magnets [77–79]. Note that in the crossover regime interference between magnetic vortices and three-dimensional ordering fluctuations masks the pure BKT scenario. Therefore the model fails to describe the domain close to T_m (see Fig. 4). The Korringa slope $m = 6.0(5)$ Oe/K was found to be nearly isotropic and independent from frequency within the error bars. Similar values of the Korringa slope were reported in other Eu-based FeAs superconductors [33,71,72].

Thus, as a conclusion of ESR measurements, the BKT transition at low temperatures proves the two dimensionality of Eu-magnetism decoupled from the conduction electrons of the FeAs layers, while the Koringa behavior for high temperatures signifies the three dimensionality of the metallic phase.

B. Resistivity and critical fields

The temperature dependence of the normalized electrical resistivity is shown in Fig. 5. Even though the material is metallic, as other 1144-type and 122-type superconductors, it shows a convex curvature instead of a normal linear metallic behavior. This feature is associated with multiband effects in hole doped materials where carriers in different bands show different mobilities for different temperatures [80,81]. The residual resistivity ratio (RRR) was determined as $R_{300K}/R_{40K} = 14.5$ and hence indicates good crystal quality [Fig. 5(a)]. This value is similar to the value reported in Ref. [48]. No finite resistance occurs at or below the temperature of the magnetic order. The inset depicts the single crystal under investigation. A sharp superconducting transition occurs at $T_c = 36.5$ K. The superconducting transition temperature window is only about 0.4 K. No reentrance behavior is observable at the ordering temperature of the Eu^{2+} magnetic moments at $T_m = 15$ K, as a return to the normal state at this temperature. This shows the unique behavior of this compound due to the strong decoupling of the magnetic and superconducting sublattices. This is in contrast to some Eu containing 122-iron-based superconductors which show a reentrance behavior [21,82,83]. These findings are in a good agreement with those in Ref. [48].

In order to investigate the superconducting anisotropy, the superconducting transition was studied in various fields applied within the ab plane and along the c axis. The shift of the transition in magnetic fields up to 14 T applied in the ab plane and along the c axis are depicted in Figs. 5(b) and 5(c). In both measurements the current was applied within the ab plane. The superconducting transition is only suppressed by a few Kelvin in a field of 14 T. As an example for $B||c$ the transition shifts to roughly 34 K. The suppression is more efficient if the field is applied perpendicular to the c axis but the anisotropy is rather small. For both directions, a negative magnetoresistance was observed in the normal conducting region. The origin of the negative magnetoresistance is due to a suppression of the electron scattering by spin fluctuations. A similar behavior was found in $EuFe_2As_2$ [84,85].

The lower critical field B_{c1} was determined using magnetization measurements for various temperatures. The corresponding phase diagram is shown in Fig. 6. At lower temperatures, $B_{c1}(T)$ displays a discontinuous temperature dependence below 20 K, which is likely related to the strong increase of the magnetic susceptibility on approaching the magnetic phase transition [cf. Fig. 1(b)]. As shown later by ARPES, the superconducting gap is not influenced by the magnetic ordering. Thus, here we ignore Eu ordering and describe the temperature dependence of the lower critical field by the generic expression [86,87]:

$$\frac{B_{c1}(T)}{B_{c1}(0)} = \frac{\lambda^2(0)}{\lambda^2(T)} = 1 + 2\int_{\Delta}^{\infty} \frac{\partial f}{\partial E} \frac{E}{\sqrt{E^2 - \Delta^2(T)}} dE, \quad (3)$$

where $B_{c1}(T)/B_{c1}(0) = \rho_s(T)$ and $\rho_s(T)$ is the normalized superfluid density. $\lambda(T)$ is the penetration depth of superconductivity. Here $f(E)$ is the Fermi distribution function and $\Delta(T) = \Delta(0)\tanh[1.82(1.018(T_c/T - 1)]^{0.51}$ is the superconducting gap for an isotropic superconductor. Following our data, $\Delta(0)$ is 8.62(4) meV for both crystallographic directions. These values are in agreement with our estimated ARPES measurement results (Fig. 11). The fit values of $B_{c1}^{c}(0) = 128.3(4)$ mT and $B_{c1}^{ab}(0) = 33.6(2)$ mT. The transition temperatures are $T_c^{ab} = 36.48(8)$ K and $T_c^{c} = 37.53(4)$ K.

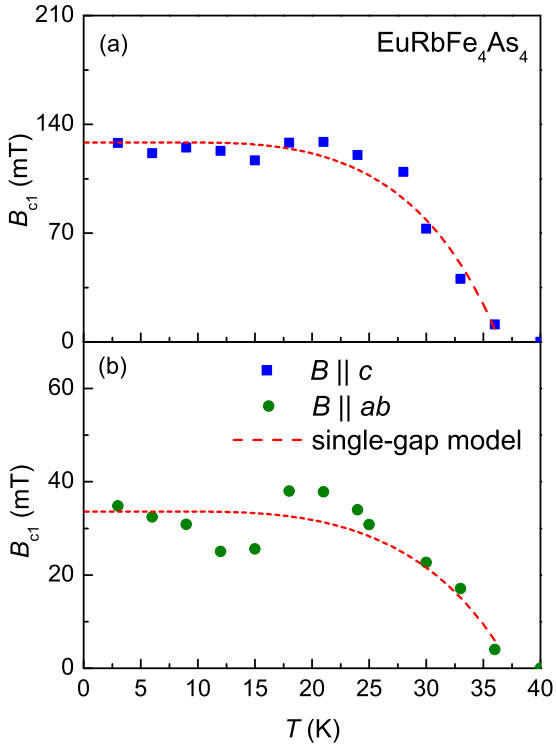

FIG. 6. The phase diagram of the lower critical field applied along the c axis (b) and in the ab plane (a), respectively. The lower critical fields show distinct minima at roughly 15 K which corresponds to the magnetic ordering temperature. In addition, both exhibit bumps in the temperature range between 20 and 30 K. The dot lines show a single-gap model [Eq. (3)] usually used in isotropic superconductors.

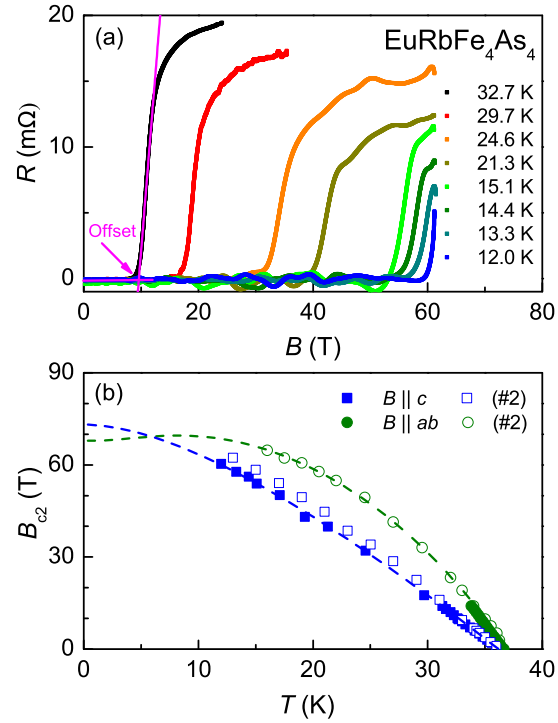

FIG. 7. (a) Field-dependent resistivity measurements carried out by pulsed magnet for fields $H||c$ up to 63 T at different temperatures. The offset shows the criteria of the determination of T_c. (b) Phase diagram of the upper critical field of $EuRbFe_4As_4$. The data can be satisfactorily fitted using the Werthamer-Helfand-Hohenberg (WHH) model (the fit curves are shown as dashed lines). For the spin-orbit parameter $\lambda_{so} = 0$, the fit indicates $B_{c2}(0) \approx 73$ T and $T_c = 36.19(5)$ K with $\alpha = 0$. For $B||ab$, one obtains $B_{c2}(0) \approx 68$ T and $T_c = 36.83(7)$ K with $\alpha = 1.9$ from sample No. 2 data of Ref. [50] (open symbols).

Very recent optical spectroscopy studies of single crystals of $EuRbFe_4As_4$ [49] showed a weak manifested dip in $\rho_s(T)$ for $10 \leqslant T \leqslant 15$ K. Currently, scanning Hall microscopy data [61] exhibit a remarkable suppression of $\rho_s(T)$ near T_m due to the correlated magnetic fluctuations, as suggested earlier by Koshelev in Ref. [53]. The data in Ref. [61] are modeled reasonably by assuming the zero-temperature superconductivity gap $\Delta(0) = 2$ meV. Although our ARPES values of $\Delta(0)$ (Fig. 11) and that value given in Ref. [49] are larger, the suggested value of $\Delta(0)$ is in good agreement with the findings in $Ba_{0.6}K_{0.4}Fe_2As_2$. [88]. In this compound, a pronounced kink was observed in the $B_{c1}(T)$ data. Following the adapted form of Eq. (3), two superconducting energy gaps came out from the fit results [89]: a small gap of about 2 meV and a large gap of approximately 9 meV. These results supported the previous ARPES observations in $Ba_{0.6}K_{0.4}Fe_2As_2$ [90] and were consistent with later electronic band structure calculations [91].

On the other hand, using the two-gap model in order to fit our data does not produce any physical values. It seems that the dips around the magnetic order temperature of Eu^{2+} ions are rather due to magnetic correlations. Moreover, both ARPES and optical spectroscopic measurements were not able to resolve any second lower gap at 2 meV. [49,60].

To complete the superconducting phase diagram, the upper critical field $B_{c2}(T)$ was determined using field-dependent resistivity measurements at different temperatures below T_c in static magnetic fields up to 14 T both for $B||ab$ and $B||c$ as well as in pulsed fields up to 65 T for the latter case as shown in Fig. 7(a). On decreasing temperatures, a strong increase of the upper critical field $B_{c2}(T)$ was observed. In Fig. 7(b) the phase diagram for the upper critical field in both directions is shown. Due to the lack of our own high-field data for $B||ab$, we added recent literature data of Smylie *et al.* [50] (sample No. 2), which are in satisfactory agreement with our data for $B||c$ and nicely match the slope of our data for $B||ab$.

For $B||c$, the data exhibit a concave curvature which is well described by the Werthamer-Helfand-Hohenberg model [92] [see Fig. 7(b)] with spin-orbit coupling $\lambda = 0$ and Maki parameter $\alpha = 0$. The extrapolated upper critical field value at zero temperature $B^c_{c2}(0) \approx 73$ T is close to that value obtained in Ref. [50]. According to Tinkham [86], with this value one can estimate the zero-temperature coherence length within the ab plane as $\xi^{ab}(0) = [\Phi_0/2\pi B^c_{c2}(0)]^{0.5} \approx 2.12$ nm where Φ_0 is the magnetic flux quantum. For $B||ab$ fitting the data completed by those of Smylie *et al.* [50] yields $B^{ab}_{c2}(0) \approx 68$ T with $\lambda = 0$ and $\alpha = 1.9$. This gives $\xi^c(0) = \Phi_0/2\pi B^{ab}_{c2}(0)\xi^{ab}(0) \approx 2.28$ nm. Both values of ξ are nearly equal. As $\xi^c(0)$ is larger than the thickness of the superconducting layer $d = c/2 \approx 0.66$ nm, this indicates that superconductivity in this compound does not split into

superconductivity of individual FeAs layers and, hence, possesses a three-dimensional and not a two-dimensional character [93].

The anisotropy factor $\gamma = B_{c2}^{ab}(0)/B_{c2}^{c}(0)$ is found to be 0.93. This value is smaller than that found in the nearly isotropic superconductor $Ba_{0.6}K_{0.4}Fe_2As_2$ [94]. It implies that $EuRbFe_4As_4$ is also a nearly isotropic, i.e., a three-dimensional superconductor. This is a consequence of its Fermi-surface topology in contrast to several compounds of 1111-type, which exhibit a considerable amount of anisotropy [95] like in high-temperature superconducting cuprates [96] and organic superconductors, [97] for which the Fermi surfaces are rather two-dimensional.

Furthermore, one can roughly estimate the ratio of ξ^{ab} to the mean-free path l using a single-band anisotropic Drude formula $l = \hbar(3n\pi^2\sqrt{\epsilon})^{1/3}/n\rho_n e^2$ where $\rho_n \approx 20\ \mu\Omega$.cm at $T = T_c$, $n = 1.25 \times 10^{21}$ cm^{-3}, and $\sqrt{\epsilon} = 1/\gamma \approx 0.76$. One obtains $l \approx 50$ nm which is much larger than $\xi^{ab}(0)$ satisfying the clean limit condition.

Finally, we focus on the meaning of the Maki parameter defined by the relative strength of orbital and spin pair breaking as $\alpha = \sqrt{2}B_{c2}^{orb}(0)/B^P(0)$ which accounts for the effects of both spin-orbit scattering and Pauli paramagnetism in a weakly coupled superconductor [98]. In the Pauli paramagnetic limiting case, the so-called Chandrasekhar-Clogston limit is determined by the superconducting energy gap Δ as [99,100]

$$B^P(0) = \Delta/\sqrt{g}\mu_B = 1.76k_B T_c/\sqrt{g}\mu_B, \tag{4}$$

where $g = 2$ is the Landé factor for a free electron. In the case of a multiband scenario by using the value of a narrow Drude gap $\Delta \approx 1.59k_B T_c$ (5 meV) at 4 K given in Ref. [49], which is close to the estimated value of the middle hole pocket (see Fig. 11), this leads to $B^P(0) \approx 61$ T. On the other hand, the orbital limit of the upper critical field is estimated in the framework of the WHH theory from the slope of the upper critical field close to T_c as [92]

$$B_{c2}^{orb}(0) = -0.69T_c[dB_{c2}(T)/dT]_{T=T_c}. \tag{5}$$

The gradient values $[dB_{c2}^{ab,c}(T)/dT]_{T=T_c}$ are found to be -4.5 T/K and 2 T/K, respectively, which are in the same order of the value found in polycrystalline $EuRbFe_4As_4$ [36]. Thus, it yields $B_{c2}^{orb}(0) \approx 113$ T and 50 T for $B||ab$ and $B||c$, respectively. The value of $B_{c2}^{orb}(0)$ in the ab plane predominates that calculated for $B^P(0)$ by a factor $\alpha \approx 2.6$ (compare with α values of several iron-based superconductors given in Ref. [95]). For $B||c$, $\alpha \approx 1.2$ is slightly larger than the value of the single-band FFLO instability threshold ($\alpha \approx 1$) [11]. Although these values of α determined only from the slope at T_c are somewhat larger than those obtained from the fitting of the complete data set, both evaluations indicate that the pair breaking effect of the magnetic field is rather dominated by orbital effects than by the Pauli limit for $B||ab$, while $B^P(0)$ exceeds $B_{c2}^{orb}(0)$ for the magnetic field applied along the c axis and, therefore, the paramagnetic limiting effect should become dominant in the characterization of the actual upper critical field [101].

As a conclusion of these considerations, we see that the upper critical field in $EuRbFe_4As_4$ is nearly isotropic.

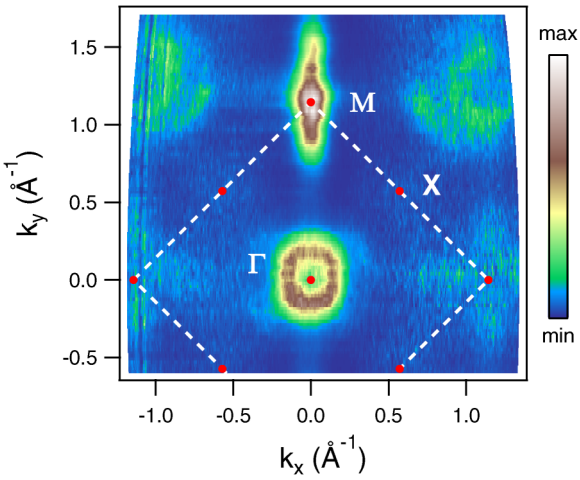

FIG. 8. ARPES Fermi surface map of $EuRbFe_4As_4$ obtained by integrating the photoemission intensity in a 15-meV window centered at E_F. The data were measured at a temperature of 20 K using vertically polarized photons with an energy of 87 eV.

These findings agree with those results found generally in related iron-based superconductors. Furthermore, the spin-paramagnetic effect is the dominant pair-breaking mechanism for the magnetic field applied along the crystallographic c axis, while the spin-orbit effect dominates in the ab plane.

C. ARPES

In Fig. 8 we present the Fermi surface (FS) of $EuRbFe_4As_4$, measured by ARPES [102] using vertically polarized photons with an energy $h\nu = 87$ eV. The map shows the FS of the inner hole pocket near the Γ point situated at $k_{x,y} = (0, 0)$. Due to matrix element effects [63,64] for this photon polarization, the middle hole and the outer hole pocket are not visible at the Γ point. On the other hand, in the second Brillouin zone (BZ) at the Γ point, traces of both the middle and the inner hole pockets are detected (see upper right and left corner of the figure). Near $k_{x,y} = (0, 1.2)$ Å^{-1} at the M point, the propellerlike electron pocket is visible for this photon polarization.

Cuts measured at a temperature of 1.5 K with photons with $h\nu = 28$ eV are depicted in Fig. 9. Near Γ along the Γ-M direction, corresponding in Fig. 8 to the vertical k_y axis, the dispersion of the hole pockets is visible. The map in Fig. 9(a) was measured using vertically polarized photons recording spectral weight with predominantly Fe 3d(yz) character. Because of matrix element effects, only the inner hole pocket is visible. Using horizontally polarized photons the spectral weight with predominantly Fe 3d(xz) character of the inner hole pocket is detected [see Fig. 9(b)] [63]. Some intensity of an additional band appears above 20 meV in the center of the BZ.

The dashed red lines in Fig. 9 are BCS-like dispersions described by $E(k) = (\epsilon(k)^2 + \Delta^2)^{\frac{1}{2}}$. The normal state dispersion $\epsilon(k)$ was determined from a parabola fit to the maxima in momentum distribution curves (MDC) in the energy range $0.012 < E < 0.03$ eV, sufficiently far away from the superconducting gap. The maxima, in turn, were obtained from

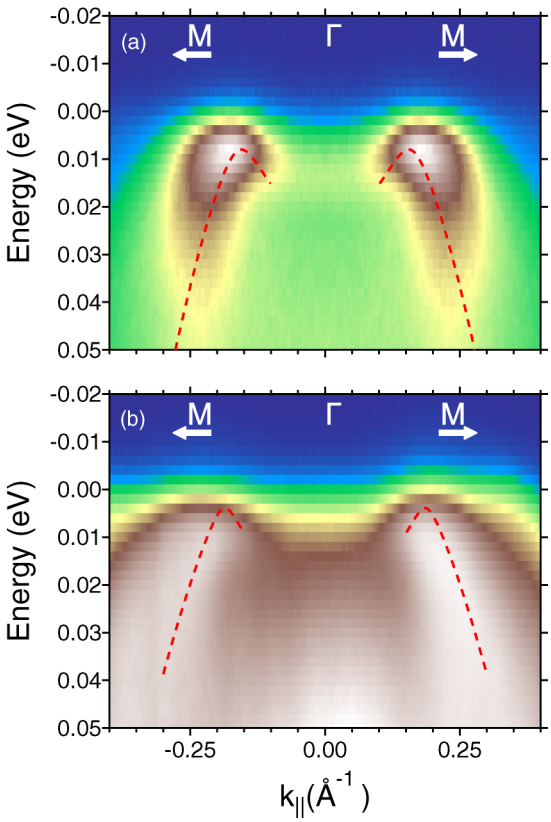

FIG. 9. ARPES energy-momentum distribution maps (MDCs) of $EuRbFe_4As_4$ measured along the $\Gamma - M$ direction at a temperature of 1.5 K using photons with an energy of 28 eV. The intensity scale is the same as in Fig. 8. The red dashed lines correspond to a parabolic dispersion together with a Bogoliubov-like back dispersion at low energies. The parameters for these curves were derived from an analysis of the ARPES data (see text). (a) Inner hole pocket measured with vertically polarized photons. (b) Middle hole pocket measured with horizontally polarized photons.

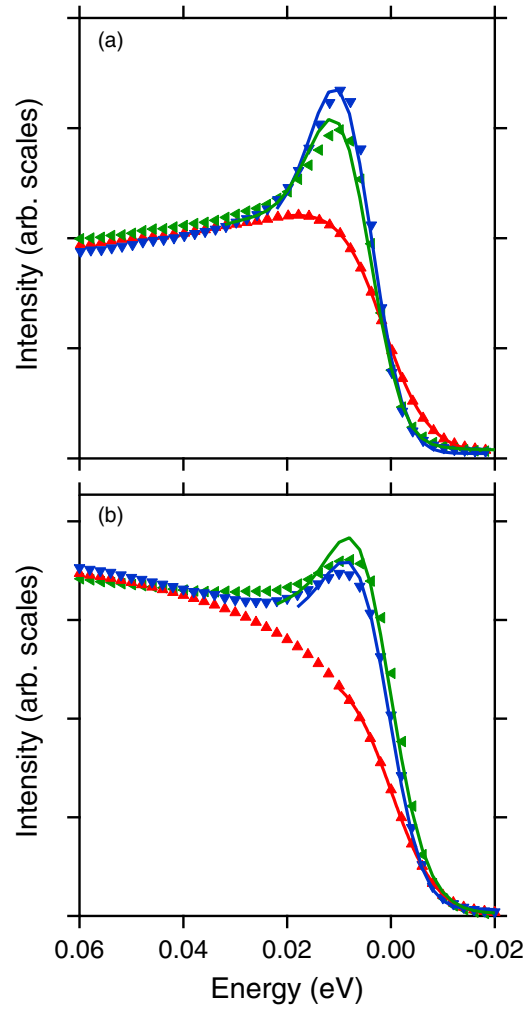

FIG. 10. ARPES density of states in $EuRbFe_4As_4$ derived from a k summation of data similar to those presented in Fig. 9. Data measured at temperatures 1.5 K, 20 K, and 50 K are marked by blue, green, and red symbols, respectively. Solid lines are results from fits. For the normal state data measured at 50 K a Fermi edge is used. For the data measured in the superconducting state a Dynes function is used for the fit of the data. (a) Data from the inner hole pocket. (b) Data from the outer hole pocket.

Lorentzian fits to the MDCs. The gap values Δ were derived from the Dynes fits (cf. Fig. 9). There are clear differences in the dispersion between the inner and the middle hole pockets, similar to other electron and hole doped ferropnictides, and related compounds [103–109]. The effective mass of the inner hole pocket is ≈30 percent smaller than that of the middle hole pocket. Different Fermi wave vectors $k_F = 0.149$ Å^{-1} and 0.195 Å^{-1} for the inner and the middle hole pocket, respectively, were determined from measurements in the normal state at 50 K. As expected for an orthorhombic system, the top of the two bands with xy ad yz symmetry should be degenerate at $k_y = k_{||} = 0$. Actually the fits yield within error bars the same energy $E = 0.023$ eV for the top of the two bands.

In Fig. 10 we present the density of states $\rho(E)$, derived from the k summation of the cuts shown in Fig. 9 over a range of $k_F \pm 0.05$ Å^{-1}. Figure 10(a) shows data of the inner hole pocket, while Fig. 10(b) shows data from the middle hole pocket. In both panels data for the temperatures 1.5 K, 20 K, and 50 K are presented. Normal state data are fitted with a Fermi function. The superconducting gaps Δ are derived from data measured in the superconducting state by fitting with a Dynes function [110]:

$$\rho(E) = \Re \frac{E - i\Gamma_S}{((E - i\Gamma_S)^2 - \Delta^2)^{0.5}}. \quad (6)$$

Here Γ_S is the finite width caused by the imaginary part of the order parameter. Furthermore, we convoluted the Dynes function with a Gaussian, the width of which is determined by the finite energy resolution. For the inner hole pocket we obtain Δ values of about 8 meV, while for the middle hole pocket we obtain values about 4 meV. Slightly higher values for the gap of the inner and the middle hole pocket were reported in Ref. [60]. Considerably higher gap values, but with the same difference, were derived for $Ba_{0.6}K_{0.4}Fe_2As_2$ [111]. For Γ_S we receive values around 0.06 meV typical of strong coupling superconductors [110].

The central ARPES result is that within error bars we detect for both hole pockets no change of the

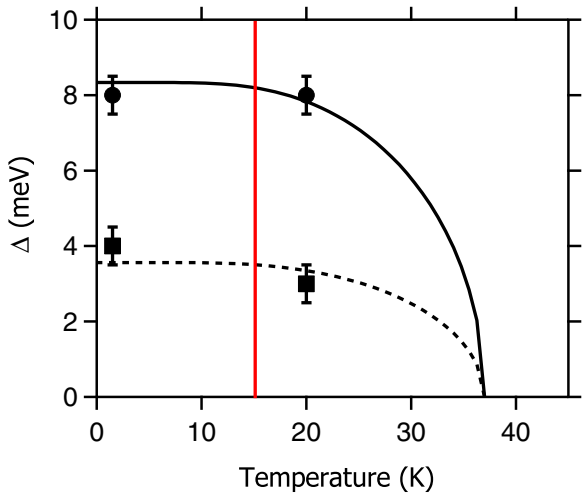

FIG. 11. Experimental results of the superconducting gap as a function of temperature derived from the fits presented in Fig. 10 using data measured along the k_y direction. (Filled circles) Data from the inner hole pocket; (squares) data from the middle hole pocket. The solid and the dashed lines present the temperature dependence expected from the weak coupling BCS theory using a superconducting transition temperature $T_c = 36.5$ K. The red line marks the ferromagnetic transition temperature $T_m = 15$ K of the Eu^{2+} system.

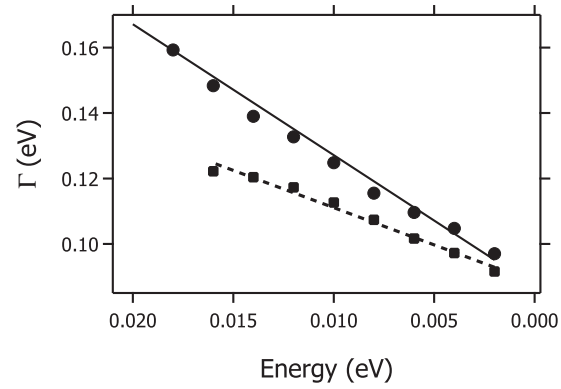

FIG. 12. Experimental results of the energy-dependent scattering rates $\Gamma(E)$ for the inner (closed circles) and the middle (squares) hole pocket, derived from measurements of the spectral weight along the k_y axis in the normal state at $T = 50$ K. The solid and the dashed lines are linear fits to the data of the inner and the middle hole pockets, respectively.

superconducting gap between $T = 1.5$ and 20 K although the magnetic order of the Eu^{2+} ions sets in at $T_m = 15$ K. For the inner hole pocket we obtain the gap values $\Delta(T = 1.5\text{ K}) = 8.0 \pm 0.5$ meV and $\Delta(T = 20\text{ K}) = 8.2 \pm 0.5$ meV. For the middle hole pocket we receive $\Delta(T = 1.5\text{ K}) = 3.9 \pm 0.5$ meV and $\Delta(T = 20\text{ K}) = 3.0 \pm 0.5$ meV. This is illustrated in Fig. 11, where we show the temperature dependence of the superconducting gaps Δ for the inner and the middle hole pocket. In this figure, we have also added the temperature dependence of the superconducting gap expected within the weak-coupling BCS theory [112]. This curve is justified because there are several studies of the temperature dependence of the superconducting order parameter of iron-based superconductors which indicate a BCS-like behavior [113–117].

In our analysis, in particular for the normal state, we assume that there is no pseudogap in iron-based superconductors. Although there are some studies which claim to have detected a pseudogap [118,119], the majority of the investigations conclude from ARPES [116,117,120,121] and from STS [122,123] that there is no pseudogap in iron-based superconductors.

Looking in Fig. 9(a) to the dispersion of the inner hole pocket, a strong decay of the spectral weight is detected with increasing energy. This indicates a rapid increase of the scattering rate $\Gamma(E)$ as a function of energy due to strong correlation effects. These are probably caused by a coupling between the hole and the electron pockets via spin fluctuation excitations, which is the most popular model for $s^{\pm}$ superconductivity for iron based superconductivity [124,125]. A considerably less dramatic reduction of the width at constant energy is realized for the middle hole pocket [see Fig. 9(b)]. Although the evaluation of scattering rates in $EuRbFe_4As_4$ is much more difficult than in other iron-based superconductors because of the rapid broadening of the spectral weight for the inner hole pocket and the presence of other bands in the case of the middle hole pocket, we present in Fig. 12 some data of $\Gamma(E)$ close to the Fermi level. The data were obtained from the momentum width multiplied by the velocity, both derived from Lorentzian fits of MDCs [126]. For both hole pockets, a linear in energy non-Fermi-liquid increase is detected. The slopes $\beta = d\Gamma/dE$ for the inner and the middle hole pockets are 4.0 and 2.3, respectively. As discussed in several previous investigations on other Fe-based superconductors [104,105,108,109] we also observe in $EuRbFe_4As_4$ scattering rates with slopes β well above the Planckian limit [127] $\beta = 1$. Finally we mention that we obtain for both pockets, as expected, the same elastic scattering contribution $\Gamma(0) = 0.088$ eV.

The strong difference of the scattering rates of the inner and the middle hole pockets, having Fe $3d$ (yz) and (xz) orbital character along the k_y axis, respectively, is a remarkable result. It indicates that these scattering processes, which probably mediate superconductivity, are related to the symmetry of sections of the electron pocket which have the same orbital character. The difference in the scattering rates has been observed in several other iron-based superconductors such as NaFeAs [104], LiFeAs [108], and electron and hole doped $BaFe_2As_2$ [105,109]. This observation was predicted from RPA calculations, which pointed out that intraorbital scattering rates are larger than interorbital scattering rates. We also mention semiphenomenological calculations on the basis of a coupling of the electrons to spin fluctuations, obtained for the inner hole pocket of $Ba_{0.6}K_{0.4}Fe_2As_2$ in the normal state. They obtained for the imaginary part of the self-energy a value for the inner hole pocket which is about twice as big as that for the middle hole pocket [128]. Because the sections having a specific orbital character in the two hole pockets are rotated by 90°, the coupling of the inner hole pocket to the electron pockets is considerably larger than that of the middle hole pocket [129,130]. However, this difference is in strong contrast to combined density functional plus dynamical mean-field theory (DFT + DMFT) calculations, which do not

show any differences between the scattering rates for these two pockets [108]. As mentioned above, in the standard model for $s^{\pm}$ superconductivity in iron-based superconductors the strength of the superconducting order parameter should be related to the strength of the interhole scattering rates. In this way, we can explain the larger superconducting gap for the inner hole pocket when compared to the middle hole pocket (see Fig. 11).

As discussed already above, the central result of the ARPES measurements is that the superconducting order parameter does not change when the magnetic order of the Eu^{2+} system appears. This shows the unique behavior of $EuRbFe_4As_4$ due to the strong decoupling of the magnetic and superconducting sublattices.

IV. SUMMARY

We have successfully synthesized high-quality single crystals of $EuRbFe_4As_4$. We have performed high-field magnetotransport and ESR and ARPES measurements in order to understand the interplay between the topological magnetic order of localized Eu^{2+} ions and nearly isotropic superconductivity of the itinerant electrons of the Fe 3*d* band.

ESR results for both in-plane and out-of-plane exhibit a reduced density of states on the Fermi level compared to a typical metal. It means that a smaller amount of conduction electrons of FeAs layers is scattered by localized magnetic moments of Eu^{2+}. Previous ESR study of $EuFe_2As_2$ also pointed out that the density of conduction electrons is significantly reduced in the SDW ground state [70]. On the other hand, vortex dynamics of Eu^{2+} moments exists only for $H||c$ and is completely absent for $H||ab$, although Eu^{2+} magnetic moments favor aligning within the *ab* plane. As a result, the BKT phase transition is suppressed in the *ab* plane by the strong ferromagnetism. It implies that weak ferromagnetism is required to realize a BKT phase transition.

The anisotropy in the upper critical field of $EuRbFe_4As_4$ is very small at low temperature. It reflects the three-dimensional character of the Fermi surface as expected for this class of materials. ARPES measurements show that in the presence of magnetic order on the Eu site, the superconducting order parameter does not change. It implies that there is strong decoupling of magnetic and superconducting sublattices.

As a final conclusion, the analysis of all experimental data of this peculiar system demonstrates that superconductivity is decoupled from the Eu^{2+} magnetic moments. This seems to be a direct result of the topological protection of the Eu^{2+} magnetic order from conduction electrons of the FeAs layers.

ACKNOWLEDGMENTS

This work was supported by the German Research Foundation Project No. 477107745057 (TRR80) and by the Freistaat Bayern through the Programm für Chancengleichheit für Frauen in Forschung und Lehre. M.H. and H.-A.K.v.N. acknowledge funding within the joint RFBR-DFG research project Contracts No. 19-51-45001 and No. KR2254/3-1. We acknowledge the support of the HLD at HZDR, a member of the European Magnetic Field Laboratory (EMFL).

[1] V. Ginzburg, Zh. Eksp. Teor. Fiz. **31**, 202 (1956) [Sov. Phys. JETP **4**, 153 (1957)].
[2] B. T. Matthais, H. Suhl, and Corenzwit, Phys. Rev. Lett. **1**, 92 (1958).
[3] P. W. Anderson and H. Suhl, Phys. Rev. **116**, 898 (1959).
[4] W. A. Fertig, D. C. Johnston, L. E. DeLong, R. W. McCallum, M. B. Maple, and B. T. Matthias, Phys. Rev. Lett. **38**, 987 (1977).
[5] M. Ishikawa and O. Fischer, Solid State Commun. **23**, 37 (1977).
[6] I. Felner, U. Asaf, Y. Levi, and O. Millo, Phys. Rev. B **55**, R3374(R) (1997).
[7] C. Bernhard, J. L. Tallon, Ch. Niedermayer, Th. Blasius, A. Golnik, E. Brücher, R. K. Kremer, D. R. Noakes, C. E. Stronach, and E. J. Ansaldo, Phys. Rev. B **59**, 14099 (1999).
[8] S. S. Saxena, P. Agarwal, K. Ahilan, F. M. Grosche, R. K. W. Haselwimmer, M. J. Steiner, E. Pugh, I. R. Walker, S. R. Julian, P. Monthoux, G. G. Lonzarich, A. Huxley, I. Sheikin, D. Braithwaite, and J. Flouquet, Nature (London) **406**, 587 (2000).
[9] D. Aoki, A. Huxley, E. Ressouche, D. Braithwaite, J. Flouquet, J.-P. Brison, E. Lhotel, and C. Paulsen, Nature (London) **413**, 613 (2001).
[10] A. I. Buzdin, Rev. Mod. Phys. **77**, 935 (2005).
[11] A. I. Larkin and Y. N. Ovchinnikov, Zh. Eksp. Teor. Fiz. **47**, 1136 (1964) [Sov. Phys. JETP **20**, 762 (1965)].
[12] P. Fulde and R. A. Ferrell, Phys. Rev. **135**, A550 (1964).
[13] V. Zdravkov, A. Sidorenko, G. Obermeier, S. Gsell, M. Schreck, C. Müller, S. Horn, R. Tidecks, and L. R. Tagirov, Phys. Rev. Lett. **97**, 057004 (2006).
[14] D. Lenk, M. Hemmida, R. Morari, V. I. Zdravkov, A. Ullrich, C. Müller, A. S. Sidorenko, S. Horn, L. R. Tagirov, A. Loidl, H.-A. Krug von Nidda, and R. Tidecks, Phys. Rev. B **93**, 184501 (2016).
[15] Y. Kamihara, T. Watanabe, M. Hirano, and H. Hosono, J. Am. Chem. Soc. **130**, 3296 (2008).
[16] S. R. Saha, N. P. Butch, K. Kirshenbaum, J. Paglione, and P. Y. Zavalij, Phys. Rev. Lett. **103**, 037005 (2009).
[17] G.-H. Cao, Z. Ma, C. Wang, Y. Sun, J. Bao, S. Jiang, Y. Luo, C. Feng, Y. Zhou, Z. Xie, F. Hu, S. Wei, I. Nowik, I. Felner, L. Zhang, Z.-A. Xu, and F.-C. Zhang, Phys. Rev. B **82**, 104518 (2010).
[18] Y. K. Luo, H. Han, S. Jiang, X. Lin, Y. Li, J. Dai, G.-H. Cao, and Z.-A. Xu, Phys. Rev. B **83**, 054501 (2011).
[19] Y. Xiao, Y. Su, M. Meven, R. Mittal, C. M. N. Kumar, T. Chatterji, S. Price, J. Persson, N. Kumar, S. K. Dhar, A. Thamizhavel, and Th. Brueckel, Phys. Rev. B **80**, 174424 (2009).
[20] H. S. Jeevan, Z. Hossain, D. Kasinathan, H. Rosner, C. Geibel, and P. Gegenwart, Phys. Rev. B **78**, 052502 (2008).
[21] W. H. Jiao, W.-H. Jiao, Q. Tao, J.-K. Bao, Y.-L. Sun, C.-M. Feng, Z.-A. Xu, I. Nowik, I. Felner, and G.-H. Cao, Europhys. Lett. **95**, 67007 (2011).
[22] W. H. Jiao, I. Felner, I. Nowik, and G.-H. Cao, J. Supercond. Nov. Magn. **25**, 441 (2012).

[23] Z. Ren, X. Lin, Q. Tao, S. Jiang, Z. Zhu, C. Wang, G.-H. Cao, and Z.-A. Xu, Phys. Rev. B **79**, 094426 (2009).

[24] S. Nandi, W. T. Jin, Y. Xiao, Y. Su, S. Price, W. Schmidt, K. Schmalzl, T. Chatterji, H. S. Jeevan, P. Gegenwart, and Th. Brückel, Phys. Rev. B **90**, 094407 (2014).

[25] Z. Ren, Q. Tao, S. Jiang, C. Feng, C. Wang, J. Dai, G.-H. Cao, and Z. Xu, Phys. Rev. Lett. **102**, 137002 (2009).

[26] S. Jiang, H. Xing, G. Xuan, Z. Ren, C. Wang, Z.-A. Xu, and G.-H. Cao, Phys. Rev. B **80**, 184514 (2009).

[27] A. Ahmed, M. Itou, S. Xu, Z.-A. Xu, G.-H. Cao, Y. Sakurai, J. Penner-Hahn, and A. Deb, Phys. Rev. Lett. **105**, 207003 (2010).

[28] I. Nowik, I. Felner, Z. Ren, G.-H. Cao, and Z. A. Xu, J. Phys. Condens. Matter **23**, 065701 (2011).

[29] D. Wu, G. Chanda, H. S. Jeevan, P. Gegenwart, and M. Dressel, Phys. Rev. B **83**, 100503(R) (2011).

[30] H. S. Jeevan, D. Kasinathan, H. Rosner, and P. Gegenwart, Phys. Rev. B **83**, 054511 (2011).

[31] S. Zapf, D. Wu, L. Bogani, H. S. Jeevan, P. Gegenwart, and M. Dressel, Phys. Rev. B **84**, 140503(R) (2011).

[32] J. Munevar, H. Micklitz, M. Alzamora, C. Argüllo, T. Goko, F. L. Ning, A. A. Aczel, T. Munsie, T. J. Williams, G. F. Chen, W. Yu, G. M. Luke, Y. J. Uemura, and E. Baggio-Saitovitch, Solid State Commun. **187**, 18 (2014).

[33] M. Hemmida, H.-A. Krug von Nidda, A. Günther, A. Loidl, A. Leithe-Jasper, W. Schnelle, H. Rosner, and J. Sichelschmidt, Phys. Rev. B **90**, 205105 (2014).

[34] S. Yu. Grebenchuk, Zh. A. Devizorova, I. A. Golovchanskiy, I. V. Shchetinin, G.-H. Cao, A. I. Buzdin, D. Roditchev, and V. S. Stolyarov, Phys. Rev. B **102**, 144501 (2020).

[35] A. Iyo, K. Kawashima, T. Kinjo, T. Nishio, S. Ishida, H. Fujihisa, Y. Gotoh, K. Kihou, H. Eisaki, and Y. Yoshida, J. Am. Chem. Soc. **138**, 3410 (2016).

[36] K. Kawashia, T. Kinjo, T. Nishio, S. Ishida, H. Fujihisa, Y. Gotoh, K. Kihou, H. Eisaki, Y. Yoshida, and A. Iyo, J. Phys. Soc. Jpn. **85**, 064710 (2016).

[37] Y. Liu, Y.-B. Liu, Z.-T. Tang, H. Jiang, Z.-C. Wang, A. Ablimit, W.-H. Jiao, Q. Tao, C.-M. Feng, Z.-A. Xu, and G.-H. Cao, Phys. Rev. B **93**, 214503 (2016).

[38] Z. Wang, C. He, Z. Tang, S. Wu, and G.-H. Cao, Sci. China Mater. **60**, 83 (2017).

[39] J.-K. Bao, K. Willa, M. P. Smylie, H. Chen, U. Welp, D. Y. Chung, and M. G. Kanatzidis, Cryst. Growth Des. **18**, 3517 (2018).

[40] K. Iida, Y. Nagai, S. Ishida, M. Ishikado, N. Murai, A. D. Christianson, H. Yoshida, Y. Inamura, H. Nakamura, A. Nakao, K. Munakata, D. Kagerbauer, M. Eisterer, K. Kawashima, Y. Yoshida, H. Eisaki, and A. Iyo, Phys. Rev. B **100**, 014506 (2019).

[41] Zh. Devizorova, S. Mironov, and A. Buzdin, Phys. Rev. Lett. **122**, 117002 (2019).

[42] Zh. Devizorova, and A. Buzdin, Phys. Rev. B **100**, 104523 (2019).

[43] A. E. Koshelev, Phys. Rev. B **100**, 224503 (2019).

[44] C. Xu, Q. Chen, and C. Cao, Commun. Phys. **2**, 16 (2019).

[45] F. Nejadsattari, M. A. Albedah, and Z. M. Stadnik, Phil. Mag. **100**, 894 (2020).

[46] Y. Liu, Y.-B. Liu, Y.-L. Yu, Q. Tao, C.-M. Feng, and G.-H. Cao, Phys. Rev. B **96**, 224510 (2017).

[47] D. E. Jackson, D. VanGennep, W. Bi, D. Zhang, P. Materne, Y. Liu, G.-H. Cao, S. T. Weir, Y. K. Vohra, and J. J. Hamlin, Phys. Rev. B **98**, 014518 (2018).

[48] M. P. Smylie, K. Willa, J.-K. Bao, K. Ryan, Z. Islam, H. Claus, Y. Simsek, Z. Diao, A. Rydh, A. E. Koshelev, W.-K. Kwok, D. Y. Chung, M. G. Kanatzidis, and U. Welp, Phys. Rev. B **98**, 104503 (2018).

[49] V. S. Stolyarov, A. Casano, M. A. Belyanchikov, A. S. Astrakhantseva, S. Y. Grebenchuk, D. S. Baranov, I. A. Golovchanskiy, I. Voloshenko, E. S. Zhukova, B. P. Gorshunov, A. V. Muratov, V. V. Dremov, L. Y. Vinnikov, D. Roditchev, Y. Liu, G.-H. Cao, M. Dressel, and E. Uykur, Phys. Rev. B **98**, 140506(R) (2018).

[50] M. P. Smylie, A. E. Koshelev, K. Willa, R. Willa, W.-K. Kwok, J.-K. Bao, D. Y. Chung, M. G. Kanatzidis, J. Singleton, F. F. Balakirev, H. Hebbeker, P. Niraula, E. Bokari, A. Kayani, and U. Welp, Phys. Rev. B **100**, 054507 (2019).

[51] L. Xiang, S. L. Bud'ko, J.-K. Bao, D. Y. Chung, M. G. Kanatzidis, and P. C. Canfield, Phys. Rev. B **99**, 144509 (2019).

[52] K. Willa, R. Willa, J.-K. Bao, A. E. Koshelev, D. Y. Chung, M. G. Kanatzidis, W.-K. Kwok, and U. Welp, Phys. Rev. B **99**, 180502(R) (2019).

[53] A. E. Koshelev, K. Willa, R. Willa, M. P. Smylie, J.-K. Bao, D. Y. Chung, M. G. Kanatzidis, W.-K. Kwok, and U. Welp, Phys. Rev. B **100**, 094518 (2019).

[54] S. Holenstein, B. Fischer, Y. Liu, N. Barbero, G. Simutis, Z. Shermadini, M. Elender, P. K. Biswas, R. Khasanov, A. Amato, T. Shiroka, H.-H. Klauss, E. Morenzoni, G.-H. Cao, D. Johrendt, and H. Luetkens, arXiv:1911.4325.

[55] Y.-B. Liu, Y. Liu, Y.-W. Cui, Z. Ren, and G.-H. Cao, J. Phys. Condens. Matter **32**, 175701 (2020).

[56] K. Willa, M. P. Smylie, Y. Simsek, J.-K. Bao, D. Y. Chung, M. G. Kanatzidis, W.-K. Kwok, and U. Welp, Phys. Rev. B **101**, 064508 (2020).

[57] V. K. Vlasko-Vlasov, U. Welp, A. E. Koshelev, M. Smylie, J.-K. Bao, D. Y. Chung, M. G. Kanatzidis, and W.-K. Kwok, Phys. Rev. B **101**, 104504 (2020).

[58] V. S. Stolyarov, K. S. Pervakov, A. S. Astrakhantseva, I. A. Golovchanskiy, D. V. Vyalikh, T. K. Kim, S. V. Eremeev, V. A. Vlasenko, V. M. Pudalov, A. A. Golubov, E. V. Chulkov, and D. Roditchev, J. Phys. Chem. Lett. **11**, 9393 (2020).

[59] V. A. Vlasenko, K. S. Pervakov, and S. U. Gavrilkin, Supercond. Sci. Technol. **33**, 084009 (2020).

[60] T. K. Kim, K. S. Pervakov, D. V. Evtushinsky, S. W. Jung, G. Poelchen, K. Kummer, V. A. Vlasenko, V. M. Pudalov, D. Roditchev, V. S. Stolyarov, D. V. Vyalikh, V. Borisov, R. Valentí, A. Ernst, S. V. Eremeev, and E. V. Chulkov, arXiv:2008.0736.

[61] D. Collomb, S. J. Bending, A. E. Koshelev, M. P. Smylie, L. Farrar, J.-K. Bao, D. Y. Chung, M. G. Kanatzidis, W.-K. Kwok, and U. Welp, Phys. Rev. Lett. **126**, 157001 (2021).

[62] W. R. Meier, T. Kong, S. L. Bud'ko, and P. C. Canfield, Phys. Rev. Materials **1**, 013401 (2017).

[63] J. Fink, S. Thirupathaiah, R. Ovsyannikov, H. A. Durr, R. Follath, Y. Huang, S. de Jong, M. S. Golden, Y. Z. Zhang, H. O. Jeschke, R. Valenti, C. Felser, S. Dastjani Farahani, M. Rotter, and D. Johrendt, Phys. Rev. B **79**, 155118 (2009).

[64] S. Moser, J. Electron Spectrosc. Relat. Phenom. **214**, 29 (2017).

[65] S. E. Barnes, Adv. Phys. **30**, 801 (1981).
[66] F. J. Owens, Physica C **353**, 265 (2001).
[67] J. P. Joshi and S. V. Bhat, J. Magn. Reson. **168**, 284 (2004).
[68] C. Kittel, Phys. Rev. **73**, 155 (1948).
[69] J. Korringa, Physica **16**, 601 (1950).
[70] E. Dengler, J. Deisenhofer, H.-A. Krug von Nidda, S. Khim, J. S. Kim, K. H. Kim, F. Casper, C. Felser, and A. Loidl, Phys. Rev. B **81**, 024406 (2010).
[71] N. Pascher, J. Deisenhofer, H.-A. Krug von Nidda, M. Hemmida, H. S. Jeevan, P. Gegenwart, and A. Loidl, Phys. Rev. B **82**, 054525 (2010).
[72] H.-A. Krug von Nidda, S. Kraus, S. Schaile, E. Dengler, N. Pascher, M. Hemmida, M. J. Eom, J. S. Kim, H. S. Jeevan, P. Gegenwart, J. Deisenhofer, and A. Loidl, Phys. Rev. B **86**, 094411 (2012).
[73] R. H. Taylor, Adv. Phys. **24**, 681 (1975).
[74] V. Berezinskii, Zh. Eksp. Teor. Fiz. **61**, 1144 (1971) [Sov. Phys. JETP **34**, 610 (1972)].
[75] J. M. Kosterlitz and D. J. Thouless, J. Phys. C **6**, 1181 (1973).
[76] J. M. Kosterlitz, J. Phys. C **7**, 1046 (1974).
[77] M. Heinrich, H.-A. Krug von Nidda, A. Loidl, N. Rogado, and R. J. Cava, Phys. Rev. Lett. **91**, 137601 (2003).
[78] S. O. Demokritov, M. M. Kreines, V. I. Kudinov, and S. V. Detra, Zh. Eksp. Teor. Fiz. **95**, 2211 (1989) [Sov. Phys. JETP **68**, 1277 (1989)].
[79] P. Gaveau, J. P. Boucher, L. P. Regnault, and Y. Henry, J. Appl. Phys. **69**, 6228 (1991).
[80] A. A. Golubova, O. V. Dolgovb, A. V. Borisb, A. Charnukhab, D. L. Sunb, C. T. Linb, A. F. Shevchunc, A. V. Korobenkoc, M. R. Truninc, and V. N. Zverev, JETP Lett. **94**, 333 (2011).
[81] B. Shen, H. Yang, Z.-S. Wang, F. Han, B. Zeng, L. Shan, C. Ren, and H.-H. Wen, Phys. Rev. B **84**, 184512 (2011).
[82] N. Kurita, M. Kimata, K. Kodama, A. Harada, M. Tomita, H. S. Suzuki, T. Matsumoto, K. Murata, S. Uji, and T. Terashima, Phys. Rev. B **83**, 214513 (2011).
[83] U. B. Paramanik, D. Das, R. Prasad, and Z. Hossain, J. Phys.: Condens. Matter **25**, 265701 (2013).
[84] S. Jiang, Y. Luo, Z. Ren, Z. Zhu, C. Wang, X. Xu, Q. Tao, G.-H. Cao, and Z. Xu, New J. Phys. **11**, 025007 (2009).
[85] T. Terashima, N. Kurita, A. Kikkawa, H. S. Suzuki, T. Matsumoto, K. Murata, and S. Uji, J. Phys. Soc. Jpn. **79**, 103706 (2010).
[86] M. Tinkham, *Introduction to Superconductivity*, 2nd ed. (McGraw-Hill, New York, 1996).
[87] A. Carrington and F. Manzano, Physica C **385**, 205 (2003).
[88] C. Ren, Z.-S. Wang, H.-Q. Luo, H. Yang, L. Shan, and H.-H. Wen, Phys. Rev. Lett. **101**, 257006 (2008).
[89] M.-S. Kim, J. A. Skinta, T. R. Lemberger, W. N. Kang, H.-J. Kim, E.-M. Choi, and S.-I. Lee, Phys. Rev. B **66**, 064511 (2002).
[90] H. Ding, P. Richard, K. Nakayama, K. Sugawara, T. Arakane, Y. Sekiba, A. Takayama, S. Souma, T. Sato, T. Takahashi, Z. Wang, X. Dai, Z. Fang, G. F. Chen, J. L. Luo, and N. L. Wang, Europhys. Lett. **83**, 47001 (2008).
[91] F. Wang, H. Zhai, Y. Ran, A. Vishwanath, and D.-H. Lee, Phys. Rev. Lett. **102**, 047005 (2009).
[92] N. Werthamer, E. Helfand, and P. Hohenberg, Phys. Rev. **147**, 295 (1966).
[93] Y. Izyumov and E. Kurmaev, *High*-T_c *Superconductors Based on FeAs Compounds*, 1st ed., Springer Series in Material Science Vol. 143 (Springer-Verlag, Berlin/Heidelberg, 2010).
[94] H. Q. Yuan, J. Singleton, F. F. Balakirev, S. A. Baily, G. F. Chen, J. L. Luo, and N. L. Wang, Nature (London) **457**, 565 (2009).
[95] J.-L. Zhang, L. Jiao, Y. Chen, and H.-Q. Yuan, Front. Phys. **6**, 463 (2011).
[96] S. E. Sebastian, N. Harrison, E. Palm, T. P. Murphy, C. H. Mielke, R. Liang, D. A. Bonn, W. N. Hardy, and G. G. Lonzarich, Nature (London) **454**, 200 (2008).
[97] P. A. Goddard, S. J. Blundell, J. Singleton, R. D. McDonald, A. Ardavan, A. Narduzzo, J. A. Schlueter, A. M. Kini, and T. Sasaki, Phys. Rev. B **69**, 174509 (2004).
[98] K. Maki, Phys. Rev. **148**, 362 (1966).
[99] B. S. Chandrasekhar, Appl. Phys. Lett. **1**, 7 (1962).
[100] A. M. Clogston, Phys. Rev. Lett. **9**, 266 (1962).
[101] T. Kida, T. Matsunaga, M. Hagiwara, Y. Mizuguchi, Y. Takano, and K. Kindo, J. Phys. Soc. Jpn. **78**, 113701 (2009).
[102] A. Damascelli, Z. Hussain, and Z.-X. Shen, Rev. Mod. Phys. **75**, 473 (2003).
[103] P. Richard, T. Sato, K. Nakayama, T. Takahashi, and H. Ding, Rep. Prog. Phys. **74**, 124512 (2011).
[104] J. Fink, A. Charnukha, E. D. L. Rienks, Z. H. Liu, S. Thirupathaiah, I. Avigo, F. Roth, H. S. Jeevan, P. Gegenwart, M. Roslova, I. Morozov, S. Wurmehl, U. Bovensiepen, S. Borisenko, M. Vojta, and B. Büchner, Phys. Rev. B **92**, 201106(R) (2015).
[105] J. Fink, E. D. L. Rienks, S. Thirupathaiah, J. Nayak, A.van Roekeghem, S. Biermann, T. Wolf, P. Adelmann, H. S. Jeevan, P. Gegenwart, S. Wurmehl, C. Felser, and B. Büchner, Phys. Rev. B **95**, 144513 (2017).
[106] J. Nayak, K. Filsinger, G. H. Fecher, S. Chadov, J. Minár, E. D. L. Rienks, B. Büchner, S. P. Parkin, J. Fink, and C. Felser, Proc Natl Acad Sci USA **114**, 12425 (2017).
[107] I. Avigo, S. Thirupathaiah, E. D. L. Rienks, L. Rettig, A. Charnukha, M. Ligges, R. Cortes, J. Nayak, H. S. Jeevan, T. Wolf, Y. Huang, S. Wurmehl, M. I. Sturza, P. Gegenwart, M. S. Golden, L. X. Yang, K. Rossnagel, M. Bauer, B. Büchner, M. Vojta *et al.*, Phys. Status Solidi B **254**, 1600382 (2017).
[108] J. Fink, J. Nayak, E. D. L. Rienks, J. Bannies, S. Wurmehl, S. Aswartham, I. Morozov, R. Kappenberger, M. A. ElGhazali, L. Craco, H. Rosner, C. Felser, and B. Büchner, Phys. Rev. B **99**, 245156 (2019).
[109] J. Fink, E. D. L. Rienks, M. Yao, R. Kurleto, J. Bannies, S. Aswartham, I. Morozov, S. Wurmehl, T. Wolf, F. Hardy, C. Meingast, H. S. Jeevan, J. Maiwald, P. Gegenwart, C. Felser, and B. Büchner, Phys. Rev. B **103**, 155119 (2021).
[110] R. C. Dynes, V. Narayanamurti, and J. P. Garno, Phys. Rev. Lett. **41**, 1509 (1978).
[111] K. Nakayama, T. Sato, P. Richard, Y.-M. Xu, Y. Sekiba, S. Souma, G. F. Chen, J. L. Luo, N. L. Wang, H. Ding, and T. Takahashi, Europhys. Lett. **85**, 67002 (2009).
[112] H. Muehlschlegel, Z. Phys. **155**, 313 (1957).
[113] D. V. Evtushinsky, D. S. Inosov, V. B. Zabolotnyy, A. Koitzsch, M. Knupfer, B. Büchner, M. S. Viazovska, G. L. Sun, V. Hinkov, A. V. Boris, C. T. Lin, B. Keimer, A. Varykhalov, A. A. Koryuk, and S. V. Borisenko, Phys. Rev. B **79**, 054517 (2009).
[114] S. He, J. He, W. Zhang, L. Zhao, D. Liu, X. Liu, D. Mou, Y.-B. Ou, Q.-Y. Wang, Z. Li, L. Wang, Y. Peng, Y. Liu, C. Chen,

L. Yu, G. Liu, X. Dong, J. Zhang, C. Chen, Z. Xu *et al.*, Nat. Mater. **12**, 605 (2013).

[115] M. Tortello, D. Daghero, G. A. Ummarino, V. A. Stepanov, J. Jiang, J. D. Weiss, E. E. Hellstrom, and R. S. Gonnelli, Phys. Rev. Lett. **105**, 237002 (2010).

[116] T. Shimojima, F. Sakaguchi, K. Ishizaka, Y. Ishida, T. Kiss, M. Okawa, T. Togashi, C.-T. Chen, S. Watanabe, M. Arita, K. Shimada, H. Namatame, M. Taniguchi, K. Ohgushi, S. Kasahara, T. Terashima, T. Shibauchi, Y. Matsuda, A. Chainani, and S. Shin, Science **332**, 564 (2011).

[117] Y. Zhang, Z. R. Ye, Q. Q. Ge, F. Chen, J. Jiang, M. Xu, B. P. Xie, and D. L. Feng, Nat. Phys. **8**, 371 (2012).

[118] T. Sato, S. Souma, K. Nakayama, K. Terashima, K. Sugawara, T. Takahashi, Y. Kamihara, M. Hirano, and H. Hosono, J. Phys. Soc. Jpn. **77**, 063708 (2008).

[119] H.-Y. Lui, X.-W. Jia, W.-T. Zhang, L. Zhao, J.-Q. Meng, G.-D. Liu, X.-L. Dong, G. Wu, R.-H. Liu, X.-H. Chen, Z.-A. Ren, W. Yi, G.-C. Che, G.-F. Che, N.-L. Wang, G.-L. Wang, Y. Zhou, Y. Zhu, X.-Y. Wang, Z.-X. Zhao *et al.*, Chin. Phys. Lett. **25**, 3761 (2008).

[120] D. V. Evtushinsky, D. S. Inosov, V. B. Zabolotnyy, A. Koitzsch, M. Knupfer, B. Büchner, G. L. Sun, V. Hinkov, A. V. Boris, C. T. Lin, B. Keimer, A. Varykhalov, A. A. Kordyuk, and S. V. Borisenko, New J. Phys. **11**, 055069 (2009).

[121] S. V. Borisenko, V. B. Zabolotnyy, A. A. Kordyuk, D. V. Evtushinsky, T. K. Kim, I. V. Morozov, R. Follath, and B. Büchner, Symmetry **4**, 251 (2012).

[122] Y. Yin, M. Zech, T. L. Williams, and J. E. Hoffman, Physica C **469**, 535 (2009).

[123] F. Massee, Y. K. Huang, J. Kaas, E. van Heumen, S. de Jong, R. Huisman, H. Luigjes, J. B. Goedkoop, and M. S. Golden, Europhys. Lett. **92**, 57012 (2010).

[124] I. I. Mazin, D. J. Singh, M. D. Johannes, and M. H. Du, Phys. Rev. Lett. **101**, 057003 (2008).

[125] K. Kuroki, S. Onari, R. Arita, H. Usui, Y. Tanaka, H. Kontani, and H. Aoki, Phys. Rev. Lett. **101**, 087004 (2008).

[126] T. Valla, A. V. Fedorov, P. D. Johnson, and S. L. Hulbert, Phys. Rev. Lett. **83**, 2085 (1999).

[127] J. Zaanen, SciPost Phys. **6**, 61 (2019).

[128] A. Heimes, R. Grein, and M. Eschrig, Phys. Rev. Lett. **106**, 047003 (2011).

[129] S. Graser, A. F. Kemper, T. A. Maier, H.-P. Cheng, P. J. Hirschfeld, and D. J. Scalapino, Phys. Rev. B **81**, 214503 (2010).

[130] A. F. Kemper, M. M. Korshunov, T. P. Devereaux, J. N. Fry, H. P. Cheng, and P. J. Hirschfeld, Phys. Rev. B **83**, 184516 (2011).